RESEARCH ARTICLE | MARCH 14 2025

Computational polarized holography for automatic monitoring of microplastics in scattering aquatic environments

Jianqing Huang ; Shuo Zhu ; Yuxing Li ; Chutian Wang ; Edmund Y. Lam

APL Photonics 10, 036114 (2025)
https://doi.org/10.1063/5.0245936

APL Photonics ARTICLE pubs.aip.org/aip/app

Computational polarized holography for automatic monitoring of microplastics in scattering aquatic environments

Cite as: APL Photon. 10, 036114 (2025); doi: 10.1063/5.0245936
Submitted: 30 October 2024 • Accepted: 25 February 2025 •
Published Online: 14 March 2025

View Online Export Citation CrossMark

Jianqing Huang,[1,2,3,a)] Shuo Zhu,[1] Yuxing Li,[1] Chutian Wang,[1] and Edmund Y. Lam[1,b)]

AFFILIATIONS

[1] Department of Electrical and Electronic Engineering, The University of Hong Kong, Pokfulam, Hong Kong SAR, China
[2] Key Lab of Education Ministry for Power Machinery and Engineering, School of Mechanical Engineering, Shanghai Jiao Tong University, 800 Dongchuan Road, Shanghai 200240, China
[3] School of Aerospace Engineering, Xiamen University, Xiang'an South Road, Xiang'an District, Xiamen 361005, Fujian, China

[a)] **Author to whom correspondence should be addressed:** jianqing.huang@xmu.edu.cn
[b)] **Electronic mail:** elam@eee.hku.hk

ABSTRACT

Automatic monitoring of microplastic (MP) contamination in aquatic ecosystems is crucial for effective management and mitigation strategies. However, this task presents significant challenges due to the dynamic 3D distribution of MPs and the light scattering in the aqueous phase. Traditional MP detection methods are limited in volumetric imaging and anti-scattering capability, often requiring cumbersome manual processing and analysis. In this study, we develop an integrated imaging system based on computational polarized holography, which offers unique advantages in automation, multifunctionality, and affordability. As demonstrated with proof-of-concept experiments, our system enables accurate and efficient 3D tracking of dynamic MPs across an extended detection volume, facilitating high-throughput analysis. In addition, the proposed hybrid de-scattering algorithm substantially improves image quality even when characterizing MPs in scattering milk solutions. Furthermore, an unsupervised clustering method is developed to identify and classify different MPs based on their multimodal features without the need for manual annotation. Although the experiments were implemented in the laboratory, the results demonstrate the robust monitoring efficiency and material-dependent sensitivity of our system. It opens up new opportunities for on-site continuous monitoring of MP pollution in aquatic ecosystems, contributing significantly to sustainable environmental management.

I. INTRODUCTION

Microplastic (MP) pollution has become a pressing environmental concern, particularly within aquatic ecosystems.[1–3] This pervasive issue not only undermines environmental integrity but also threatens social and economic sustainability, directly contradicting the UN Sustainable Development Goals, notably SDG3 (good health and well-being) and SDG6 (clean water and sanitation).[4] Monitoring MP contamination on-site is critical for comprehending their natural behaviors, such as spatiotemporal distribution, settlement, aggregation, migration, degradation, and interaction with micro-organisms. Such information is scarcely found in the current literature but carries significant implications for developing effective MP management and mitigation strategies. Conventional methodologies for MP assessment typically involve labor-intensive and time-consuming processes such as water sampling, complex pre-treatment procedures, and extensive laboratory analysis.[5,6] These methods frequently fail to maintain the original properties of MPs, leading to the loss of crucial information such as agglomeration behavior and biofilm interactions.[7] Optical imaging technologies have surfaced as promising solutions for long-term and high-frequency monitoring of MPs due to their versatility and non-invasive nature.[8–11]

However, on-site automatic monitoring of MPs presents considerable challenges.[12,13] The dynamic and volumetric distribution of MP particles necessitates imaging systems with superior 3D spatial resolution and adaptable computational capabilities to precisely capture their complex dynamics.[8,14] Moreover, the inherent complexity of aquatic environments, characterized by fluctuating currents and diverse habitats, further complicates the monitoring process. The scattering of light in water due to suspended micro/nano-particles (e.g., diatoms, minerals, fragments, foams, bubbles, and bacteria) and dissolved substances poses another substantial challenge, leading to image degradation and hindering precise detection and characterization of MPs.[15,16] The degradation in image quality not only affects the identification and tracking of individual MPs but also impacts the ability to distinguish MP types and quantify MP concentrations.

Currently, researchers have initiated pioneering efforts in the development of portable optical devices for *in situ* MP detection.[17–20] For example, Leonard *et al.*[21] reported a smartphone-based method to evaluate MP contamination levels, which involves isolating MPs by density separation and vacuum filtration, staining the isolated plastic polymers with Nile Red, and quantifying the stained MPs using a smartphone-based fluorescence microscope. Deng *et al.*[22] designed a prototype of polarized light scattering to distinguish sediments, MPs, and phytoplankton in seawater, showcasing the potential of optical techniques in identifying suspended particles. Recently, Ye *et al.*[23] developed a wireless portable device for analyzing labeled MP samples with quantitative fluorescence imaging. Ren *et al.*[24] suggested a pyrolysis-point discharge optical emission spectrometer for rapid plastic type identification. Although sample preparation is necessary for pyrolysis, their portable instrument simplifies the detection process. In addition, Nayak *et al.*[25] reviewed holographic imaging techniques for *in situ* aquatic particle detection, showing the great potential of holography for MP monitoring. For example, an autonomous holographic imaging system (Auto-holo) has been developed and demonstrated to work underwater with real plankton samples.[26]

The majority of these documented approaches entail discrete sampling, manual sample processing, and labor-intensive image analysis, which significantly constrain their scalability and efficiency. Typically, these methods necessitate mechanical scanning of the target volume, manual extraction of particles from the background, and visual inspection based on expert knowledge. Consequently, the automation and continuous monitoring of dynamic MPs remain largely unachieved. Moreover, the challenge of MP image degradation induced by scattering effects persists without adequate resolution in current methodologies. Some techniques attempt to mitigate this issue by reducing the detection distance through the use of thin slides and microfluidic channels or by substituting turbid water with clear water for experimental demonstrations.[13,27] Therefore, due to the intrinsic scattering effects, the applicability of these methods in authentic aquatic environments is highly questionable.

To address the challenge of automatically detecting dynamic MPs through scattering media, our research endeavors to develop an integrated imaging system that harnesses advanced optical and computational technologies. In our prior investigations,[28,29] we demonstrated that the combination of polarization and holographic imaging facilitates effective discrimination of MP materials by analyzing their optical features. In addition, we found that the polarization property of light provides significant opportunities to address the image degradation problem induced by turbid water.[30,31] We also made preliminary attempts to realize high-throughput analysis of MP particles by pumping MP suspensions into a microfluidic channel.[32] Building upon these works, this study concentrates on developing an automatic and multifunctional approach for MP monitoring. In particular, a hybrid de-scattering algorithm is proposed to tackle the scattering problem from turbid aquatic environments (simulated with diluted milk solutions). Furthermore, the feasibility of unsupervised clustering methods in automated MP identification is verified for the first time. A set of proof-of-concept experiments is implemented in the laboratory with diverse lab-prepared samples. Through rigorous experimental validation, we illustrate the efficacy of our approach in tracking and characterizing dynamic MPs in highly scattering media. We believe that our innovative solution offers a promising pathway toward reliable and efficient monitoring of MP pollution across diverse aquatic ecosystems.

II. MATERIALS AND METHODS

A. Portable imaging system

1. Optical setup

Figure 1 schematically depicts the designed portable imaging system based on computational polarized holography, including its optical configuration, prototype, and typical deployment scenario. As illustrated in Fig. 1(a), single shot polarization imaging is embedded into an in-line holographic imaging configuration, without compromising the reliability and simplicity of its original optical structure. The illumination laser beam (wavelength $\lambda = 632.8$ nm) is expanded and circularly polarized by a set of lenses (a convex lens ($f = 75$ mm), a linear polarizer, and a quarter wave plate). The polarization camera (MG-A500P-22, Crevis Tech.,

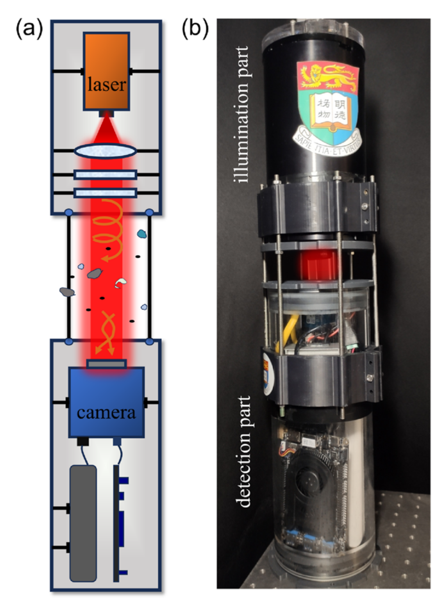

FIG. 1. Schematic diagram of the designed imaging system for on-site monitoring of MP contamination. (a) The optical configuration mainly includes a laser, lenses, a polarization camera, a mobile power supply, and a microcomputer. (b) The assembled prototype.

South Korea) is capable of simultaneously recording holographic fringes and resolving four specific polarization orientations (POs) (0°, 45°, 90°, and 135°). The spatial resolution of the image sensor is 2464 × 2056 with a square pixel size of 3.45 μm, and the equivalent pixel size of the polarimetric channels is 6.9 μm. Since no lens was equipped in the camera, the magnification in the image plane is unity. Therefore, abundant information about the dynamic particles and their surrounding scattering environment can be captured in a single exposure.[33] It enables the establishment of specific computational methods (which will be introduced in Subsection II B) to extract high-dimensional features of MPs and address the image degradation problem caused by the scattering effect.

Similar holography-based systems have been previously reported in the literature. For instance, the Auto-holo designed by Nayak *et al.*[26] has a stable structure and 3D imaging capability but cannot perform MP discrimination. Göröcs *et al.*[17] demonstrated a portable holographic imaging flow cytometer in which the water sample is pumped through the microfluidic channel for detection. In addition, other polarization-based holographic approaches have been developed. For example, Valentino *et al.*[13,34] designed a polarization-sensitive holographic microscopy for MP classification, which requires two snapshots with diagonally and anti-diagonally polarized illumination beams, respectively. Compared with these works, our system has unique advantages in low cost, simple optical configuration, automatic operation, and anti-scattering capability.

We have designed a prototype of our imaging system with a simple yet reliable mechanical and optical structure. As shown in Fig. 1(b), the assembled cylindrical prototype is ~60 cm high and 15 cm in diameter. Connection and support components are manufactured by 3D printing. The gap (i.e., the detection volume) between the illumination part and the detection part is adjustable (1–20 cm). A mobile power supply (12 V, 20 000 mA h) and a microcomputer (LattePanda 3 Delta) are assembled with the camera for image acquisition and processing. With the advantages of low cost and simple structure, our system could be flexibly deployed in diverse aquatic environments, such as oceans, lakes, and rivers. However, due to unresolved engineering issues such as long-term waterproofing and long-distance wireless data transmission, the current prototype cannot be effectively tested in natural water environments. As a result, our focus in the present work shifts to validating the system (especially the computational methods) through proof-of-principle experiments conducted in a laboratory setting.

2. Sample preparation

To validate the feasibility of our imaging system, the well-identified MP samples and simulated turbid aquatic environments are prepared. The MP particles are generated from disposable plastic bags (LDPE: low density polyethylene) and water bottles (PET: polyethylene terephthalate). In addition, we also purchase polystyrene (PS) and methyl methacrylate (PMMA) plastic materials (Xinsheng Plastic Material Company, China) for testing. All of these polymer materials are colorless, transparent or translucent, and difficult to distinguish with the naked eye. Without loss of generality, the size of MP particles ranges from 600 to 1200 μm for ease of implementation in this study. The MP samples are washed with deionized water to remove dust or other impurities. A cuboid water container with a transparent glass wall is employed to disperse these MP particles with distilled water or milk solutions. The MP suspensions are manually mixed with a glass rod before the experiment. The selection of a milk solution as a simulated scattering medium in underwater environments is driven by its consistent particle distribution, closely resembling natural water turbidity. This choice offers flexibility in regulating the scattering properties of the aqueous phase through the manipulation of milk solution concentrations. This experimental approach is widely employed in various underwater imaging investigations.[35,36] Nonetheless, natural water samples are undoubtedly more complex, containing a variety of particles such as diatoms, minerals, fragments, foams, bubbles, bacteria, and microbial biofilms. The simplified experiments conducted with milk solutions lay the groundwork for future realistic validation. To simulate dynamic particle fields, the prepared MP suspensions are perturbed by spraying water with a syringe, resulting in individual MP particles rotating, tumbling, or moving randomly. Since no pumping systems or filters are used, the MP suspensions are manually updated with different types of MP samples and varying turbidity. The corresponding holograms of the dynamic and volumetric particle fields are consecutively recorded at 22 frames per second (fps).

B. Computational methods

1. Holographic reconstruction

Digital holography has been extensively applied in characterizing various particles.[37–39] The holographic interference fringes recorded by the image sensor can be expressed as

$$h(u,v) = |E_O(u,v) + E_R(u,v)|^2, \tag{1}$$

where $h(u,v)$ is the intensity of the hologram on the imaging plane with coordinates (u,v), E_O is the diffracted wave of the object, and E_R indicates the un-diffracted plane wave. By numerically back propagating (BP) the hologram to a specific reconstruction plane with coordinates (x,y,z), the complex optical field of the target object $\Gamma(x,y,z)$ can be retrieved. As a popular holographic reconstruction method, the angular spectrum algorithm[40] is adopted in this work,

$$\Gamma(x,y,z) = \mathscr{F}^{-1}\left\{\mathscr{F}\{h\} \times \exp\left(-i\frac{2\pi z}{\lambda}\sqrt{1-\lambda^2 f_x^2 - \lambda^2 f_y^2}\right)\right\}, \tag{2}$$

where $\mathscr{F}$ is the Fourier transform, and f_x and f_y are the transverse spatial frequencies. Then, the intensity of the refocused image can be obtained by $I = |\Gamma|^2$, and the phase $\varphi = \tan^{-1}\frac{\mathrm{Im}(\Gamma)}{Re(\Gamma)}$, where "Im" and "Re" represent the imaginary and real parts of Γ, respectively. Since the in-focus depth of each particle is unknown, volumetric reconstruction is performed among the whole detection volume $z_r \in [20, 60]$ mm with a small depth interval $\Delta z = 0.2$ mm.

2. Automatic particle segmentation and tracking

To automatically determine particles' shape, size, and 3D location from the stack of reconstructed images, a two-step particle segmentation algorithm is proposed in this work. First, adaptive image binarization is performed in the synthetic grayscale image $I_{gy}(x,y) = \min I(x,y,z_r)$ using an "imbinarize" function from MATLAB. The segmentation threshold is adaptively selected based on the local first-order statistics of the intensity in the neighborhood of each pixel. As a result, a local region for each particle is efficiently estimated for the next step. For each region of interest (ROI) with coordinates (k, l), a precise particle edge is extracted by considering both the local distributions of the hybrid grayscale intensity $I_{gy}(ROI)$ and the hybrid grayscale gradient $T_{gd}(ROI) = \max T(x, y, z_r)$, where $T(x, y, z_r) = |I(x, y, z_r) \otimes S_x|^2 + |I(x, y, z_r) \otimes S_y|^2$ is the image gradient calculated with horizontal and vertical Sobel kernels (S_x, S_y). Briefly, the particle edge $v(k, l)$ is determined when the mean edge gradient reaches the maximum,

$$v(k,l) = \arg\max_{b\in(0,1)} \frac{\sum_{k,l\in ROI} \mathscr{S}\{\mathscr{G}_b\{I_{gy}(k,l)\}\} \cdot T_{gd}(k,l)}{\sum_{k,l\in ROI} \mathscr{S}\{\mathscr{G}_b\{I_{gy}(k,l)\}\}}, \quad (3)$$

where symbol $\mathscr{S}$ denotes an operation to extract the exterior edge pixels of the binarized image $(\mathscr{G}_b\{I_{gy}(k,l)\})$ with the binarization threshold $b \in (0, 1)$, using an "edge" function from MATLAB. Therefore, with the well-identified particle edge, it is easy to obtain the in-plane shape, size, area, perimeter, and location of each particle. Note that specific morphological operations are also included in these segmentation procedures, such as corrosion, expansion, and filling image holes. In addition, based on the sharpness criterion, an integrated focus metric is established to determine the particle's in-focus depth z_f,

$$z_f = \arg\max_{z_r} \sum_{k,l\in ROI} v(k,l) \cdot T(k,l,z_r) + \alpha \cdot \mathscr{D}\{T(k,l,z_r)\}, \quad (4)$$

where symbol $\mathscr{D}$ denotes an operation to calculate the standard deviation and α is a relaxation factor for balancing the two independent parts. Compared with conventional focus metrics, which are often based on a single feature, the integrated focus metric offers more robustness for detecting irregular MP particles.[37]

Consequently, with all particles in each frame successfully segmented and accurately localized, an automatic 3D particle tracking algorithm can be established for monitoring dynamic particle fields. Given the positions of two particles P_1 and P_2 at different frames, their Euclidean distance $d(P_1, P_2) = \sqrt{(x_1 - x_2)^2 + (y_1 - y_2)^2 + (z_1 - z_2)^2}$ is employed to measure the distances of arbitrary pair particles. By minimizing the sum of the pair distances of all particles between two consecutive frames,

$$\kappa^* = \arg\min_{\kappa} \sum_{n=1}^{N} \sum_{m=1}^{M} d(P_n, P_m)\kappa(m,n), \quad (5)$$

where N and M are the numbers of particles in the two frames (n and m are the indices), the optimal particle matching κ^* can be created between each frame pair. After all particle matching is done through multiple frames, several particle trajectories can be extracted with explicit track beginnings and ends (i.e., the particles enter and leave the observation window), which enables us to analyze the time-resolved rotation and translation of particles.

3. Hybrid de-scattering algorithm

To tackle the image degradation problem caused by scattering aquatic environments, a hybrid de-scattering algorithm, termed "H3P," is proposed by leveraging the scattering characteristics in polarization orientation (PO), propagation reconstruction (PR), and planar distribution (PD). When the circularly polarized illumination laser beam passes through a scattering medium, the photons detected by the image sensor consist of ballistic photons and scattered photons. First, the ballistic photons, which carry object information, can maintain their original polarization states,[30,41] while the unwanted scattered photons have arbitrary polarization states due to multiple scattering. Hence, the four simultaneously captured holograms with different POs provide an effective strategy to suppress the diverse scattered photons by averaging. To take full advantage of the diversity in POs of scattered photons, a lot of synthetic holograms can be generated by polarization reassignment in each pixel,

$$h_s(u,v) = \mathscr{R}\{h_0, h_{45}, h_{90}, h_{135}\}, \quad (6)$$

where symbol $\mathscr{R}$ denotes an operation for each pixel to randomly select only one PO from the four candidates. Thus, these synthetic holograms increase the diversity of scattered photons while keeping a similar and correlated distribution of ballistic photons. Most of the holographic fringes are well preserved in the synthetic holograms, which ensures the following accurate back propagation reconstruction. Similar strategies that suppress image noise by introducing noise diversity from different optical dimensions are also named "multi-look" or "diversity technique" in the literature.[42–44] Their noise reduction performance is strongly related to the number of looks and the correlation between looks.

Second, when experiencing random scattering, the scattered photons tend to lose their coherence,[45,46] while the majority of ballistic photons can maintain their coherence property and thereby have a larger depth of focus. Taking this unique characteristic into consideration, it is possible to further suppress scattered photons during the propagation reconstruction process. Each synthetic hologram is back propagating to a series of reconstruction planes around its in-focus plane $(z = z_f)$. Then, averaging these quasi-focused reconstructed images can effectively neutralize the incoherent scattered photons. The mathematical expression of this strategy is

$$\bar{\Gamma}_s(x,y,z_f) = \frac{1}{Q} \sum_{z=z_f-\frac{Q}{2}\delta z}^{z_f+\frac{Q}{2}\delta z} \Gamma_s(x,y,z), \quad (7)$$

where Q is the number of quasi-focused images, δz is a tiny depth variance (10 μm), and Γ_s is the reconstruction of a synthetic hologram h_s.

Finally, the planar distribution of local image structure is also beneficial for suppressing scattered photons. Due to the sparse nature of the reconstructed particle image, it is feasible to segment the image into fragments and group similar fragments for collaborative filtering.[47] Not only the fine image structure (e.g., textures and edges) shared by the grouped fragments can be preserved, but also the noise fluctuations caused by scattering can be smoothed. The Non-Local Means (NLMs)[48] and Block-Matching 3D filtering (BM3D)[49] are representative algorithms that utilize such a strategy to attenuate image noise. In this work, BM3D is employed to further enhance the image quality of holographic images. To alleviate its signal-to-noise ratio (SNR)-dependent drawback and conserve computational resources, BM3D is executed just once in the averaged reconstruction, rather than in each preliminary reconstruction. The final image obtained with our H3P algorithm can be expressed as

$$\Gamma_{H3P} = \mathscr{B}\left\{\frac{1}{S}\sum_{1}^{S}\bar{\Gamma}_s\left(x, y, z_f\right)\right\}, \tag{8}$$

where symbol $\mathscr{B}$ denotes an operation to perform BM3D using an open access algorithm,[49] and S is the number of synthetic holograms. It is worth mentioning that these three strategies utilize image features from different dimensions and jointly contribute to the final image quality improvement. The hyper-parameters in this method (e.g., Q and S) can be easily determined with calibration. The computational efficiency of the proposed algorithm is comparable with traditional de-scattering methods, i.e., ~10 seconds per frame (including polarization reassignment: 2 s, synthetic hologram reconstruction: 4 s, and collaborative filtering: 2 s).

4. Multimodal features extraction and clustering

The fusion of polarization imaging and digital holography presents a versatile platform for extracting multimodal features crucial in the classification of MPs. Within the realm of polarization, features such as the angle of polarization (AoP) and the degree of linear polarization (DoLP) stand out as valuable metrics for characterizing the birefringence and dichroism properties of MPs.[30,50] The refocused intensity maps from the polarized holograms are used to extract AoP and Dolp features. Concurrently, holography offers a dual perspective by providing both amplitude and phase data, facilitating the extraction of features such as circularity (Cir), solidity (Sol), transparency variance (TrVa), and phase smoothness (PhSm). These features play a pivotal role in discerning the morphological and refractive index characteristics of MPs.[12,51,52] Each of them is automatically calculated with the above-mentioned particle segmentation results. Detailed definitions of these distinctive features can be found in S1 of the supplementary material.

Rather than exhaustively listing all potential features for MP differentiation, we have opted to showcase these key attributes as exemplars in establishing an automated MP classification framework. This approach allows for the seamless integration of new additional features that may prove effective in future studies into our classification framework.

Clustering, a fundamental component of data mining, involves organizing data into distinct clusters according to the similarities among their features.[53] Notably, density-based clustering (DBCL) methods excel at identifying clusters of arbitrary shapes while demonstrating robust immunity to noise.[54] In the context of MP monitoring, where the number of clusters can fluctuate and new particles are continually recorded, DBCL's adaptability to these dynamic environments makes it a suitable choice for effective classification. To the best of our knowledge, the feasibility of unsupervised DBCL approaches in automatic MP discrimination has not been investigated.

With each particle represented by multimodal features, a novel MP classification framework leveraging DBCL is introduced in this study. This differs from our previous data-based approaches that require precise annotation and supervised training,[29,55] as such a clustering-based method enables more flexibility and automation. Let W denote a dynamic dataset $W = \{q_1, q_2, \ldots, q_p\}$, where each q represents an individual particle within the designed feature space (i.e., q is a normalized vector containing six feature values). If a minimum of $p_{\min}$ particles cluster within a distance of d_{eps}, these particles are recognized as dense or core points; otherwise, they are classified as outliers (noise). The estimation of these two hyper-parameters can be obtained by analyzing the dataset.[56] They are set as $p_{\min} = 20$ and $d_{\text{eps}} = 0.3$ in this study. As a result, multiple clusters representing different particle types can be delineated and dynamically updated as new particles augment the dataset. For streamlined implementation, a "dbscan" function from the MATLAB Statistics and Machine Learning Toolbox is utilized in this work. Other popular clustering algorithms, including K-means, K-medoids, spectral, and Gaussian Mixture Model (GMM), are also employed (with the known number of clusters: $K = 4$) for comparative studies.

Overall, a complete flow chart of these computational methods is illustrated in Fig. 2. In particular, the H3P de-scattering algorithm proposed in this work plays an important role in enhancing the image quality for the following tasks, such as particle counting, tracking, identification, and classification. Otherwise, the system's detection capability will deteriorate significantly due to the complex scattering environment. In addition, although the present study aims to achieve automatic MPs monitoring, a rapid or even real-time detection capability is also highly desired in the future. Boosting the computing power of the microcomputer and optimizing the connection between algorithms should be beneficial in improving computational efficiency. For example, when detecting MPs in different turbid waters, it is more efficient to adaptively adjust the iteration processes in the de-scattering, tracking, and clustering algorithms.

III. RESULTS AND DISCUSSION

A. 3D tracking of dynamic MPs

Figure 3 showcases the remarkable capabilities of our imaging system in tracking dynamic MP particles dispersed in water.

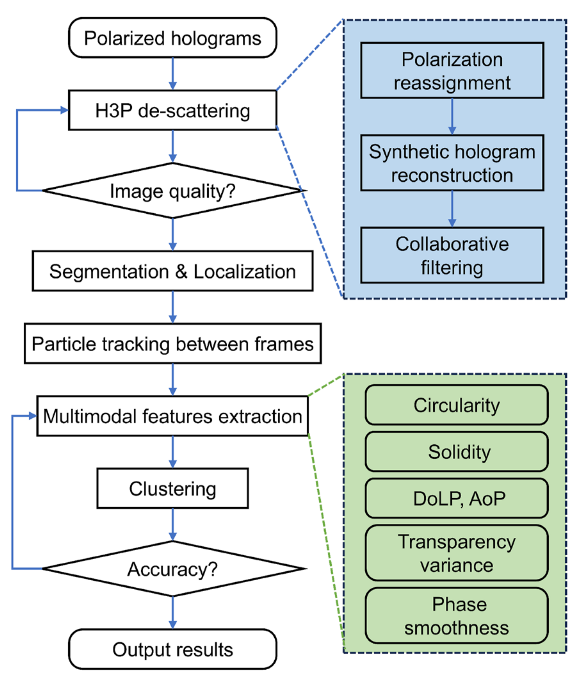

FIG. 2. Flow chart of computational methods for MPs monitoring.

A raw hologram captured in the experiments is presented in Fig. 3(a), showing intricate holographic fringes surrounding the blurred edges of particles. Leveraging sophisticated reconstruction and segmentation methods, each particle is precisely refocused to its optimal in-focus depth. For example, Fig. 3(b) presents the focus metrics evolution of two distinct particles: a fiber-shaped particle (indicated by a red arrow) located at $z_f = 35.6$ mm and a diamond-shaped PMMA particle (marked by a blue arrow) positioned at $z_f = 54.8$ mm. The narrow distribution of focus metrics underscores the system's robustness and high sensitivity across the entire depth range.

Through automated image processing, each particle is accurately refocused and segmented with sharp edges, as depicted in Fig. 3(c), enabling the quantification of essential morphological parameters such as size, area, and perimeter. These refocused particles exhibit diverse shapes and unique surface intensity distributions, crucial for distinguishing between different particle types. In addition, the system determines the 3D position of each randomly dispersed particle. Figure 3(d) showcases a 3D rendering of MP particle fields across 38 frames, providing insights into particle diameter and circularity. Further detailed reconstruction results can be explored in supporting visualization. The sharp edge features of the detected particles suggest that the segmentation and localization of particles are correct and acceptable.

In contrast to traditional microscopy methods, which often suffer from limited 2D observation capabilities and out-of-focus

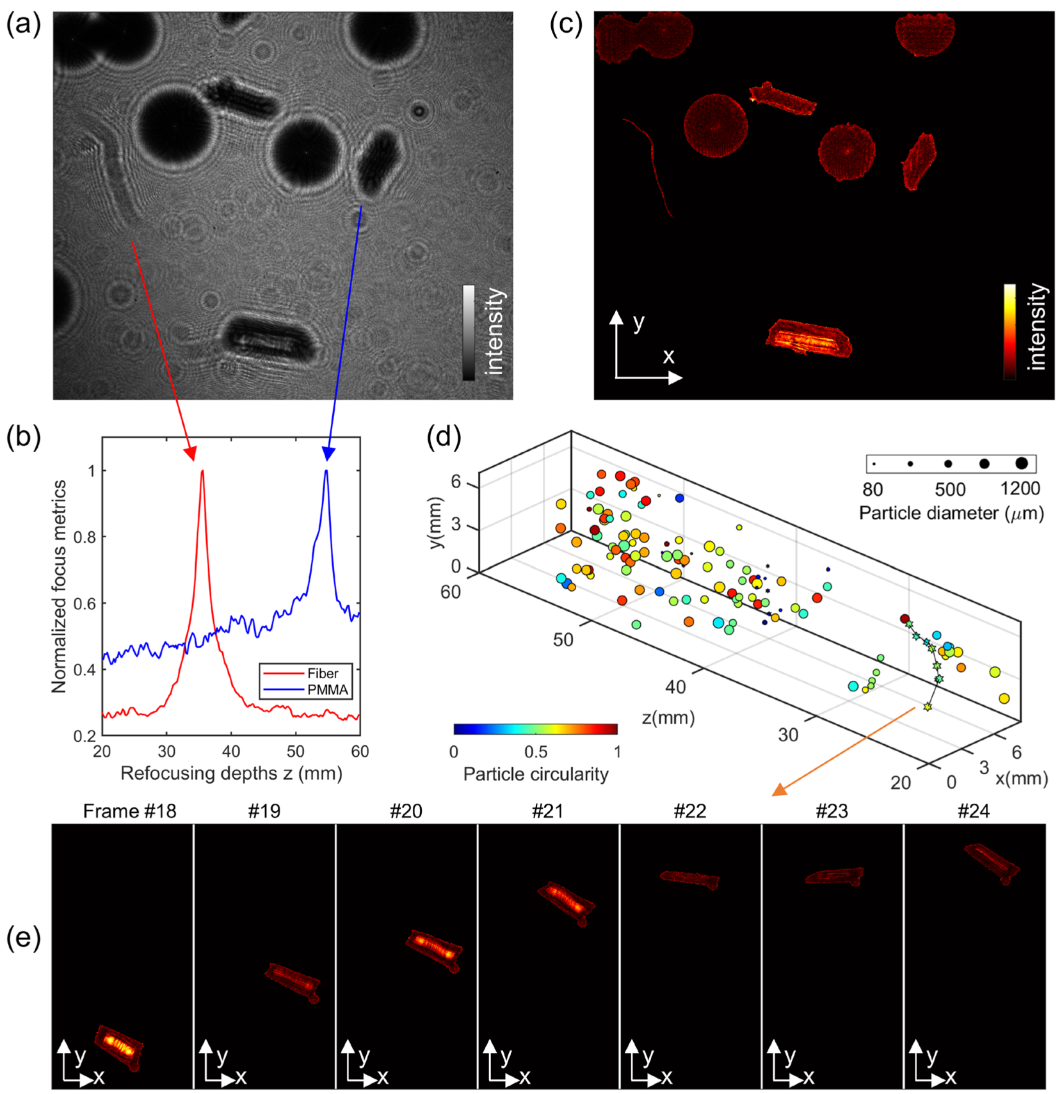

FIG. 3. Visualization of 3D reconstruction and tracking of MP particle fields. (a) The captured hologram. (b) The evolution of focus metrics of two representative particles. (c) The reconstructed particle field with each particle is sharply refocused and accurately segmented. (d) The 3D rendering of MP particle fields among 38 frames, showing particle diameter and circularity. (e) Tracking a specific MP particle among seven consecutive frames and showing the particle's projection evolution.

issues, our holographic imaging system significantly expands the depth range (from a few millimeters to tens of millimeters) for high-throughput 3D detection and dynamic tracking within large volumes. An illustrative particle trajectory spanning seven consecutive frames is highlighted with an orange arrow in Fig. 3(d), with the particle's projection evolution depicted separately in Fig. 3(e). This facilitates precise estimations of the particle's floating, rotating, and settling movements, enhancing the analysis of MP behaviors in aquatic environments (such as the aggregation and attachment behaviors between MPs and biofilms, the distribution, and the migration behaviors of MPs in water).

To evaluate the detection efficiency of our optical system and the automatic processing algorithms, three experiments (case 1–3) with increased particle concentrations were conducted, each involving around 20 frames and the number of particles in each frame ranging from 0 to 10. As demonstrated in Fig. 4, the automatic quantification results align well with manual quantification results. While a few particles may be missed when the particle number exceeds five in a single frame, the overall detection efficiency surpasses 90%, making it suitable for environmental monitoring applications where particle projection density is moderate. Adjusting the detection depth range can further optimize the system's efficiency by modulating particle projection density.

B. De-scattering performance

Before evaluating the de-scattering performance of our proposed H3P algorithm, we conducted ablation experiments to highlight the necessity of each operation. The results, detailed in S2 of the supplementary material, reveal a step-by-step improvement in image quality. These experiments underscore how the scattering characteristics in the PO, PR, and PD domains effectively aid in the suppression of scattered photons. Furthermore, the relationship between the number of synthetic holograms and the performance of noise reduction was investigated. The noise contrast[47] is adopted to quantify the performance of the multi-look method and the H3P method. The results are provided in S2 of the supplementary material. It is demonstrated that the polarization reassignment strategy can substantially generate noise diversity, which promotes the H3P method to reach near the ideal boundary of uncorrelated multiple looks.

Figure 5 demonstrates that our H3P algorithm can substantially suppress scattered photons and improve image quality when imaging MPs through scattering media. Two typical holograms of an LDPE particle (fixed on a thin glass slide) in clean water and a turbid milk solution are presented in Figs. 5(a) and 5(b), respectively. The hologram captured in water, along with its reconstructed amplitude and phase [Figs. 5(d) and 5(g)], serves as the ground truth. It becomes evident that the intensity signal of the image is significantly attenuated, and much fringe information is obscured by noise induced by scattering. Consequently, the direct retrievals of amplitude and phase without the H3P algorithm [Figs. 5(e) and 5(h)] lack texture information and suffer from poor image contrast. Conversely, as depicted in Figs. 5(f) and 5(i), the distributions of amplitude and phase reconstructed using our H3P algorithm show a well-preserved texture feature on the particle surface. In particular, intensity profiles on two line transects are extracted from Figs. 5(e) and 5(f) and are comparatively displayed in Fig. 5(c), showcasing the H3P algorithm's ability to simultaneously mitigate scattering noise and enhance image contrast. Furthermore, we quantitatively evaluate image similarity with the ground truth using the correlation coefficient (corr) and structural similarity index measure (SSIM). The results, illustrated in Fig. 5, consistently demonstrate the enhanced image quality achieved through the utilization of our H3P algorithm.

To validate the superiority of our H3P algorithm over commonly used methods, we conducted additional comparative studies involving different MP particles of varying types and sizes. As depicted in Fig. 6, the BP method only captures a rough particle outline, with both the particle's inner region and the background severely affected by noise. The compressed sensing (CS) method[46] effectively reduces background noise but compromises the texture information within the particle, leading to significant distortion. Although the BM3D method enhances image contrast to some extent, it struggles in low signal-to-noise ratio areas. In contrast, our H3P algorithm consistently outperforms these methods in image

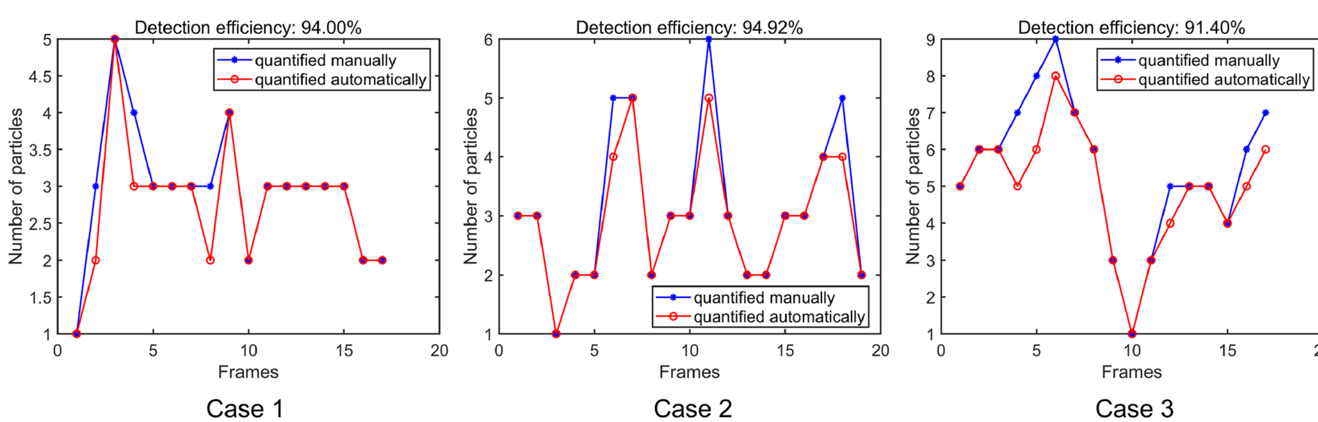

FIG. 4. Evaluation of the detection efficiency of the imaging system through manual quantification and automatic quantification. Three cases show the different particle concentrations in consecutive frames.

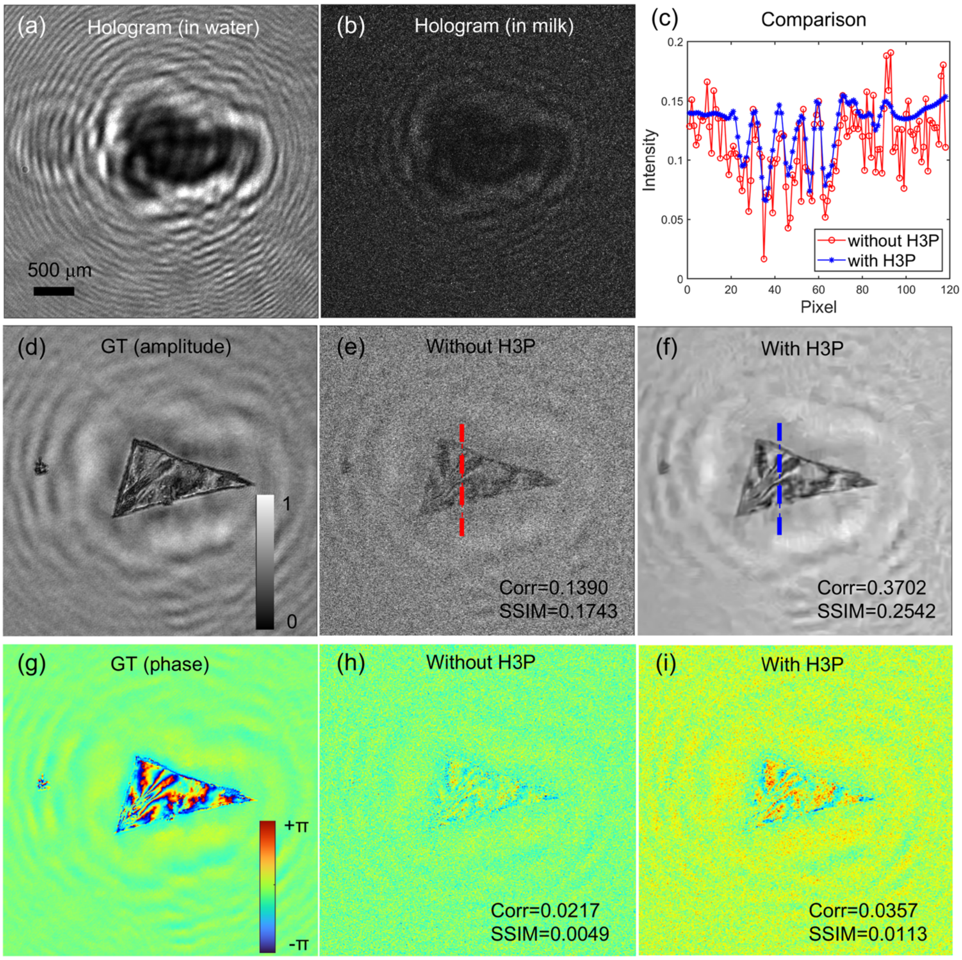

FIG. 5. Comparison between the raw image and the enhanced image using the proposed H3P de-scattering algorithm. (a) The hologram in water; (b) the hologram in a milk solution, (c) the comparison between the reconstructed amplitude distributions with or without H3P, (d)–(f) the reconstructed amplitude, and (g)–(i) the reconstructed phase. Two metrics (i.e., corr and SSIM) are used to quantify the image quality with respect to the ground truth (GT).

enhancement. In addition, we employed the naturalness image quality evaluator (NIQE[57]) to quantify the performance of these methods, where a lower score indicates better perceived quality. As depicted in Fig. 6, the results reaffirm the significant performance improvement offered by our H3P method.

Moreover, a series of experiments involving imaging the USAF resolution target with different turbid milk solutions were conducted. The milk volume concentrations were set as 0.3%, 0.5%, 0.7%, and 0.9%, respectively. The results are provided in S2 of the supplementary material. As the milk solution concentration increased, causing a gradual increase in the optical depth of the scattering medium, the system's spatial resolution degraded from 15 to 62 μm. However, with the application of the H3P algorithm, the spatial resolution of the imaging system significantly improved and remained below 30 μm. Overall, the enhanced image contrast and improved spatial resolution provided by our algorithm are pivotal for effectively characterizing diverse MPs in aquatic environments. Not only can smaller particles be effectively detected, but also more surface features can be extracted to identify different particle types.

C. Clustering-based classification of MPs

Based on the automated particle segmentation, 3D tracking, and de-scattering processes described above, a multitude of distinctive features from various MPs are efficiently extracted for detailed analysis. As illustrated in Fig. 7(a), each particle composed of different materials exhibits discernible feature distributions. For example, all MP particles exhibit sensitivity to the angle of polarization, showcasing specific and informative polarization responses. PMMA and PET particles display a significantly higher degree of linear polarization compared to the other two MP types, owing to their distinct optical anisotropy. In addition, PS particles exhibit a lower transparency variance and higher circularity, making them easily distinguishable from the rest.

In conjunction with visual inspections, a comprehensive statistical analysis was conducted on over 900 MP particles, with the feature distributions of these particles provided in S3 of the supplementary material. The distinctiveness of the four MP types is effectively demonstrated within the high-dimensional feature space. To facilitate better visualization, t-distributed Stochastic Neighbor

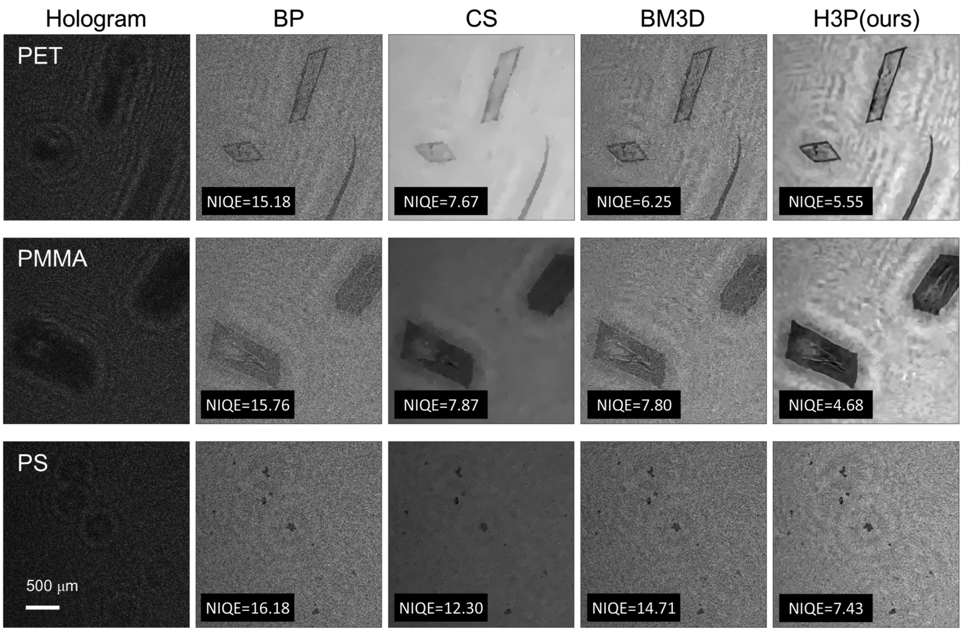

FIG. 6. Comparison among different descattering algorithms. From left to right: the scattered holograms of MPs, the reconstructed amplitude using the back propagation (BP) algorithm, the compressed sensing (CS) algorithm, the block matching 3D (BM3D) algorithm, and the proposed H3P algorithm. NIQE is the naturalness image quality evaluator, where a lower score indicates better perceived quality. Three types of MP particles (i.e., PET, PMMA, and PS) were used for demonstration.

Embedding (t-SNE)[58] is employed in this study to simplify and analyze the complex dataset. As depicted in Fig. 7(b), each type of MP displays a specific distribution in the reduced 3D virtual space. Crucially, these types can be distinctly isolated from each other, indicating the potential utility of these high-dimensional features for MP classification tasks. To further validate the efficacy of these features, six distance metrics are evaluated in t-SNE visualization (refer to S3 of the supplementary material). The results reveal that the majority of MP particles can be accurately separated, with the "correlation" metric exhibiting optimal performance. While a few particles may be mixed and could lead to misjudgments, particularly concerning PMMA and PET particles, this is deemed acceptable for conducting high-throughput and automated screening in aquatic environments. Noteworthy, a similar approach has been previously reported where the polarization features (specific parameters from the full Jones matrix) of materials have been extracted for microplastic fiber classification.[34] Both their results and the present work confirm the remarkable feasibility of polarization features. The main

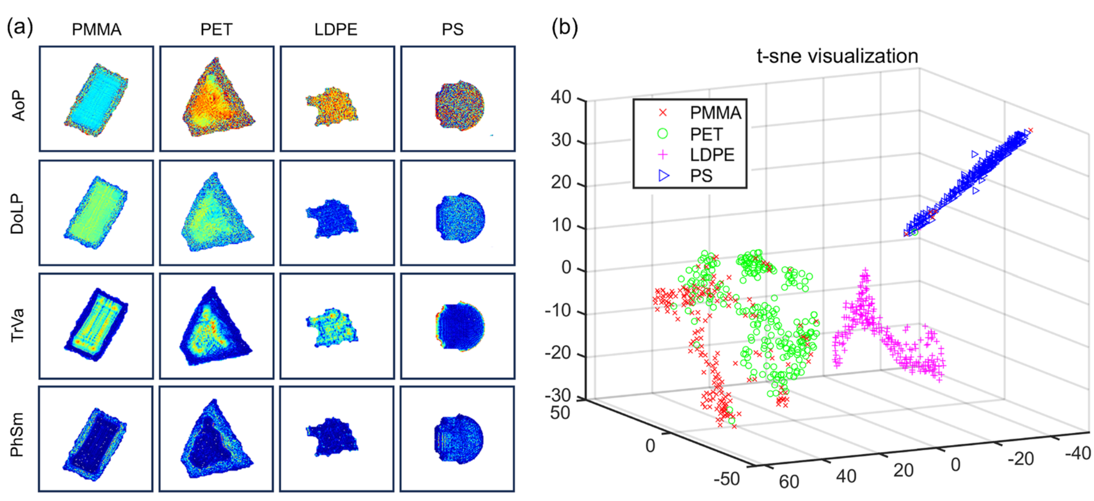

FIG. 7. Typical features and t-SNE visualization of different MP particles. (a) The Angle of Polarization (AoP), Degree of Linear Polarization (DoLP), Transparency Variance (TrVa), and Phase Smoothness (PhSm) features for PMMA, PET, LDPE, and PS particles are automatically extracted by the portable imaging system. (b) The t-SNE visualization of over 900 MP particles, showcasing four distinct MP types in a reduced 3D virtual space.

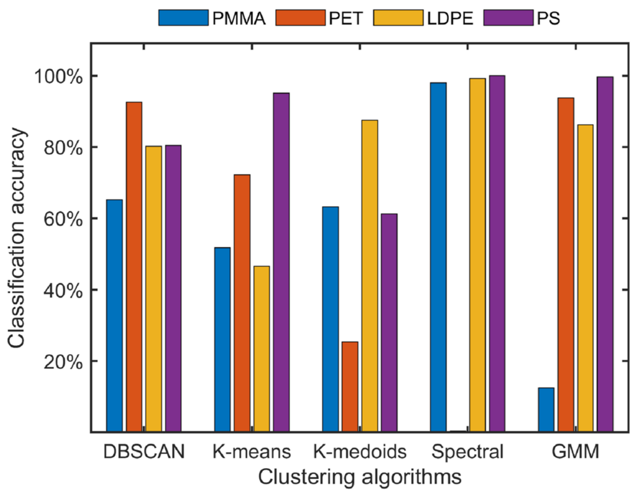

FIG. 8. Microplastic classification based on multiple features utilizing various unsupervised clustering algorithms.

difference between the two approaches is that we capture the polarization information in a single shot, while they need two recordings with different polarized illumination beams. Nevertheless, their selected features, such as eigenvectors and eigennumbers, should be valuable to strengthen our algorithm's performance, which will be included in our future research.

Subsequently, a clustering-based classification of MP particles is executed using the extracted features. Figure 8 illustrates the classification accuracy of various clustering algorithms. As anticipated, unsupervised clustering methods prove capable of automatically discriminating between different MP types. These methods obviate the need for laborious annotations or extensive training, directly segregating various MP types through the automated analysis of their multiple features. Noteworthy is the superior performance of DBSCAN (Density-Based Spatial Clustering of Applications with Noise) among the considered algorithms, showcasing an overall classification accuracy of ~80% and demonstrating exceptional proficiency in distinguishing PMMA and PET particles. Moreover, DBSCAN exhibits robust outlier detection capabilities, identifying data points that are sparsely distributed from the main cluster and prone to misclassification. Thus, future efforts will be directed toward analyzing these outliers to further enhance the system's classification accuracy.

IV. CONCLUSIONS

In summary, we design a miniaturized imaging system based on computational polarized holography for automatically detecting MP particles in water. The integration of single-shot polarization imaging and in-line holographic imaging enables the establishment of multiple functions in a single system. The developed numerical processing methods are capable of tracking dynamic MPs, enhancing image quality in scattering milk solutions, and discriminating different MP types. Although the designed prototype has been validated in laboratory settings, its compact and portable structure holds great potential for field deployment. With extensive proof-of-concept experimental validation, it is demonstrated that computational polarized holography is a simple yet powerful technique to combat the challenges of MP monitoring.

In our future research, more efforts will be devoted to testing the prototype in diverse natural environments and optimizing the computational efficiency for real-time monitoring. It is noted that realistic water samples are much more complex. For example, the natural MP particles are usually present with varying degrees of aging or are covered by microalgae and bacteria biofilms. Diverse impurities with different properties exist in natural turbid water, making the issue of light scattering more challenging to address. Therefore, the employed MP features and the corresponding numerical processing methods should be updated by analyzing the captured holographic and polarization information. As a notable contribution of the present work, computational polarized holography provides abundant optical information and versatile numerical approaches for probing MPs in scattering media. It is believed that our solution can contribute significantly to sustainable environmental management.

SUPPLEMENTARY MATERIAL

The supplementary material includes the following: the definitions and mathematical expressions of multiple features of MPs, imaging system calibration using a USAF resolution target, statistical analysis of MP features distribution, and t-SNE visualization with different distance metrics. Supporting visualization: Detailed 3D reconstruction results of 38 holographic frames.

ACKNOWLEDGMENTS

The work is supported in part by the Research Grants Council of Hong Kong (Grant Nos. GRF 17201620 and RIF R7003-21). This work was partly funded by the Hong Kong Scholars Program (Grant No. XJ2022032). Jianqing Huang appreciates the partial financial support from Shanghai Jiao Tong University.

AUTHOR DECLARATIONS

Conflict of Interest

The authors have no conflicts to disclose.

Author Contributions

Jianqing Huang: Conceptualization (lead); Formal analysis (lead); Investigation (lead); Methodology (lead); Software (lead); Writing – original draft (lead). **Shuo Zhu**: Investigation (equal); Resources (equal); Writing – review & editing (equal). **Yuxing Li**: Investigation (equal); Resources (equal); Writing – review & editing (equal). **Chutian Wang**: Investigation (equal); Resources (equal); Writing – review & editing (equal). **Edmund Y. Lam**: Funding acquisition (lead); Supervision (equal); Writing – review & editing (equal).

DATA AVAILABILITY

The data that support the findings of this study are available from the corresponding author upon reasonable request.

REFERENCES

[1]R. C. Thompson, W. Courtene-Jones, J. Boucher, S. Pahl, K. Raubenheimer, and A. A. Koelmans, "Twenty years of microplastics pollution research—what have we learned?," Science **386**, eadl2746 (2024).

[2]W. Huang and X. Xia, "Element cycling with micro(nano)plastics," Science **385**, 933–935 (2024).

[3]J. Zhao, R. Lan, Z. Wang, W. Su, D. Song, R. Xue, Z. Liu, X. Liu, Y. Dai, T. Yue, and B. Xing, "Microplastic fragmentation by rotifers in aquatic ecosystems contributes to global nanoplastic pollution," Nat. Nanotechnol. **19**, 406–414 (2024).

[4]O. Bamigboye, M. O. Alfred, A. A. Bayode, E. I. Unuabonah, and M. O. Omorogie, "The growing threats and mitigation of environmental microplastics," Environ. Chem. Ecotoxicol. **6**, 259–268 (2024).

[5]F. Stock, C. Kochleus, B. Bänsch-Baltruschat, N. Brennholt, and G. Reifferscheid, "Sampling techniques and preparation methods for microplastic analyses in the aquatic environment–A review," TrAC, Trends Anal. Chem. **113**, 84–92 (2019).

[6]X. Wang, N. Bolan, D. C. W. Tsang, B. Sarkar, L. Bradney, and Y. Li, "A review of microplastics aggregation in aquatic environment: Influence factors, analytical methods, and environmental implications," J. Hazard. Mater. **402**, 123496 (2021).

[7]B. Singh and A. Kumar, "Advances in microplastics detection: A comprehensive review of methodologies and their effectiveness," TrAC, Trends Anal. Chem. **170**, 117440 (2024).

[8]Y. Zhu, Y. Li, J. Huang, Y. Zhang, Y.-W. Ho, J. K.-H. Fang, and E. Y. Lam, "Advanced optical imaging technologies for microplastics identification: Progress and challenges," Adv. Photonics Res. **5**, 2400038 (2024).

[9]E. Y. Lam, "Artificial intelligence in biophotonics and imaging: Advancing computational reconstruction and inference," in *26th Optoelectronics and Communications Conference* (IEEE, 2021), p. T4A.2.

[10]N. Chen, L. Cao, T.-C. Poon, B. Lee, and E. Y. Lam, "Differentiable imaging: A new tool for computational optical imaging," Adv. Phys. Res. **2**, 2200118 (2023).

[11]J.-R. Lee, H. Yoo, C. C. Ciang, Y.-J. Kim, D. Kim, T. W. Teo, Z. Mahdavipour, A. Abdullah, B. E. Khoo, M. Z. Abdullah *et al.*, "Roadmap on industrial imaging techniques," Meas. Sci. Technol. **36**, 013001 (2024).

[12]D. Koestner, R. Foster, and A. El-Habashi, "On the potential for optical detection of microplastics in the ocean," Oceanography **36**, 49–51 (2023).

[13]M. Valentino, J. Běhal, V. Bianco, S. Itri, R. Mossotti, G. D. Fontana, T. Battistini, E. Stella, L. Miccio, and P. Ferraro, "Intelligent polarization-sensitive holographic flow-cytometer: Towards specificity in classifying natural and microplastic fibers," Sci. Total Environ. **815**, 152708 (2022).

[14]M. Valentino, D. G. Sirico, P. Memmolo, L. Miccio, V. Bianco, and P. Ferraro, "Digital holographic approaches to the detection and characterization of microplastics in water environments," Appl. Opt. **62**, D104–D118 (2023).

[15]M. Jian, X. Liu, H. Luo, X. Lu, H. Yu, and J. Dong, "Underwater image processing and analysis: A review," Signal Process.: Image Commun. **91**, 116088 (2021).

[16]X. Li, Y. Han, H. Wang, T. Liu, S.-C. Chen, and H. Hu, "Polarimetric imaging through scattering media: A review," Front. Phys. **10**, 815296 (2022).

[17]Z. Göröcs, M. Tamamitsu, V. Bianco, P. Wolf, S. Roy, K. Shindo, K. Yanny, Y. Wu, H. C. Koydemir, Y. Rivenson, and A. Ozcan, "A deep learning-enabled portable imaging flow cytometer for cost-effective, high-throughput, and label-free analysis of natural water samples," Light: Sci. Appl. **7**, 66 (2018).

[18]J. J. Lee, J. Kang, and C. Kim, "A low-cost TICT-based staining agent for identification of microplastics: Theoretical studies and simple, cost-effective smartphone-based fluorescence microscope application," J. Hazard. Mater. **465**, 133168 (2024).

[19]D. D. Pramanik, P. Kay, and F. M. Goycoolea, "A rapid and portable fluorescence spectroscopy staining method for the detection of plastic microfibers in water," Sci. Total Environ. **908**, 168144 (2024).

[20]Z. Wang, A. Pilechi, M. Fok Cheung, and P. A. Ariya, "*In-situ* and real-time nano/microplastic coatings and dynamics in water using nano-DIHM: A novel capability for the plastic life cycle research," Water Res. **235**, 119898 (2023).

[21]J. Leonard, H. C. Koydemir, V. S. Koutnik, D. Tseng, A. Ozcan, and S. K. Mohanty, "Smartphone-enabled rapid quantification of microplastics," J. Hazard. Mater. Lett. **3**, 100052 (2022).

[22]H. Deng, H. Wang, Z. Guo, J. Li, R. Liao, H. Li, Q. Li, and H. Ma, "Classification of suspended particles in seawater using an in situ polarized light scattering prototype," Limnol. Oceanogr.: Methods **21**, 775–789 (2023).

[23]H. Ye, X. Zheng, H. Yang, M. D. Kowal, T. M. Seifried, G. P. Singh, K. Aayush, G. Gao, E. Grant, D. Kitts *et al.*, "Cost-effective and wireless portable device for rapid and sensitive quantification of micro/nanoplastics," ACS Sens. **9**, 4662 (2024).

[24]T. Ren, Y. Li, X. Wang, Y. Deng, and C. Zheng, "Portable pyrolysis-point discharge optical spectrometer for in situ plastic polymer identification by coupling with machine learning," Environ. Sci. Technol. **58**, 2554–2563 (2024).

[25]A. R. Nayak, E. Malkiel, M. N. McFarland, M. S. Twardowski, and J. M. Sullivan, "A review of holography in the aquatic sciences: *In situ* characterization of particles, plankton, and small scale biophysical interactions," Front. Mar. Sci. **7**, 572147 (2021).

[26]A. R. Nayak, M. McFarland, J. M. Sullivan, F. Dalgleish, and L. Garavelli, "AUTOHOLO: A novel, in situ, autonomous holographic imaging system for long-term particle and plankton characterization studies in diverse marine environments," in *Ocean Sciences Meeting 2020* (AGU, 2020).

[27]V. Bianco, D. Pirone, P. Memmolo, F. Merola, and P. Ferraro, "Identification of microplastics based on the fractal properties of their holographic fingerprint," ACS Photonics **8**, 2148–2157 (2021).

[28]Y. Zhu, Y. Li, J. Huang, Y. Zhang, and E. Y. Lam, "Holographic and polarization features analysis for microplastics characterization and water monitoring," Proc. SPIE **12621**, 126210X (2023).

[29]Y. Zhu, Y. Li, J. Huang, and E. Y. Lam, "Smart polarization and spectroscopic holography for real-time microplastics identification," Commun. Eng. **3**, 32 (2024).

[30]J. Huang, Y. Zhu, Y. Li, and E. Y. Lam, "Snapshot polarization-sensitive holography for detecting microplastics in turbid water," ACS Photonics **10**, 4483–4493 (2023).

[31]J. Huang, Y. Li, Y. Zhu, and E. Y. Lam, "A field deployable imaging system for detecting microplastics in the aquatic environment," in *2024 IEEE International Symposium on Circuits and Systems (ISCAS)* (IEEE, 2024), pp. 1–5.

[32]Y. Li, Y. Zhu, J. Huang, Y.-W. Ho, J. K.-H. Fang, and E. Y. Lam, "High-throughput microplastic assessment using polarization holographic imaging," Sci. Rep. **14**, 2355 (2024).

[33]J. Huang, Y. Zhu, Y. Li, Y. Zhang, and E. Y. Lam, "Polarization-sensitive digital holography for microplastic identification through scattering media," in *Digital Holography and Three-Dimensional Imaging* (Optica Publishing Group, 2023), p. HW3D–2.

[34]J. Běhal, M. Valentino, L. Miccio, V. Bianco, S. Itri, R. Mossotti, G. Dalla Fontana, E. Stella, and P. Ferraro, "Toward an all-optical fingerprint of synthetic and natural microplastic fibers by polarization-sensitive holographic microscopy," ACS Photonics **9**, 694–705 (2022).

[35]H. Li, J. Zhu, J. Deng, F. Guo, N. Zhang, J. Sun, and X. Hou, "Underwater active polarization descattering based on a single polarized image," Opt. Express **31**, 21988–22000 (2023).

[36]Y. Li, Y. Chen, J. Zhang, Y. Li, H. Tang, and X. Fu, "A robust underwater polarization image recovery based on angle of polarization with low-rank and sparse decomposition," Opt Laser. Technol. **181**, 111669 (2025).

[37]J. Huang, W. Cai, Y. Wu, and X. Wu, "Recent advances and applications of digital holography in multiphase reactive/nonreactive flows: A review," Meas. Sci. Technol. **33**, 022001 (2021).

[38]Y. Zhang, S. H. Chan, and E. Y. Lam, "Photon-starved snapshot holography," APL Photonics **8**, 056106 (2023).

[39]Y. Zhu, H. K. A. Lo, C. H. Yeung, and E. Y. Lam, "Microplastic pollution assessment with digital holography and zero-shot learning," APL Photonics **7**, 076102 (2022).

[40]J. W. Goodman, *Introduction to Fourier Optics*, 4th ed. (W. H. Freeman Press, New York, 2017).

[41]F. Liu, X. Li, P. Han, and X. Shao, "Advanced visualization polarimetric imaging: Removal of water spray effect utilizing circular polarization," Appl. Sci. **11**, 2996 (2021).

[42]L. Rong, W. Xiao, F. Pan, S. Liu, and R. Li, "Speckle noise reduction in digital holography by use of multiple polarization holograms," Chin. Opt. Lett. **8**, 653–655 (2010).

[43] B. Redding, G. Allen, E. R. Dufresne, and H. Cao, "Low-loss high-speed speckle reduction using a colloidal dispersion," Appl. Opt. **52**, 1168–1172 (2013).

[44] V. Bianco, V. Marchesano, A. Finizio, M. Paturzo, and P. Ferraro, "Self-propelling bacteria mimic coherent light decorrelation," Opt. Express **23**, 9388–9396 (2015).

[45] S. Li and J. Zhong, "Dynamic imaging through turbid media based on digital holography," J. Opt. Soc. Am. A **31**, 480–486 (2014).

[46] H. Zhang, S. Liu, L. Cao, and D. J. Brady, "Noise suppression for ballistic-photons based on compressive in-line holographic imaging through an inhomogeneous medium," Opt. Express **28**, 10337–10349 (2020).

[47] V. Bianco, P. Memmolo, M. Paturzo, A. Finizio, B. Javidi, and P. Ferraro, "Quasi noise-free digital holography," Light: Sci. Appl. **5**, e16142 (2016).

[48] A. Buades, B. Coll, and J.-M. Morel, "Non-local means denoising," Image Process. Line **1**, 208–212 (2011).

[49] Y. Mäkinen, L. Azzari, and A. Foi, "Collaborative filtering of correlated noise: Exact transform-domain variance for improved shrinkage and patch matching," IEEE Trans. Image Process. **29**, 8339–8354 (2020).

[50] D. Koestner, R. Foster, A. El-Habashi, and S. Cheatham, "Measurements of the inherent optical properties of aqueous suspensions of microplastics," Limnol. Oceanogr. Lett. **9**, 487–497 (2024).

[51] K.-E. Peiponen, B. Kanyathare, B. Hrovat, N. Papamatthaiakis, J. Hattuniemi, B. Asamoah, A. Haapala, A. Koistinen, and M. Roussey, "Sorting microplastics from other materials in water samples by ultra-high-definition imaging," J. Eur. Opt. Soc.-Rapid Publ. **19**, 14 (2023).

[52] V. Bianco, P. Memmolo, P. Carcagnì, F. Merola, M. Paturzo, C. Distante, and P. Ferraro, "Microplastic identification via holographic imaging and machine learning," Adv. Intell. Syst. **2**, 1900153 (2020).

[53] A. E. Ezugwu, A. M. Ikotun, O. O. Oyelade, L. Abualigah, J. O. Agushaka, C. I. Eke, and A. A. Akinyelu, "A comprehensive survey of clustering algorithms: State-of-the-art machine learning applications, taxonomy, challenges, and future research prospects," Eng. Appl. Artif. Intell. **110**, 104743 (2022).

[54] P. Bhattacharjee and P. Mitra, "A survey of density based clustering algorithms," Front. Comput. Sci. **15**, 151308 (2021).

[55] Y. Zhu, C. Hang Yeung, and E. Y. Lam, "Microplastic pollution monitoring with holographic classification and deep learning," J. Phys.: Photonics **3**, 024013 (2021).

[56] M. Ester, H.-P. Kriegel, J. Sander, X. Xu *et al.*, "A density-based algorithm for discovering clusters in large spatial databases with noise," in *Proceedings of the Second International Conference on Knowledge Discovery in Databases and Data Mining*, 96 (AAAI Press, 1996), pp. 226–231.

[57] A. Mittal, R. Soundararajan, and A. C. Bovik, "Making a 'completely blind' image quality analyzer," IEEE Signal Process. Lett. **20**, 209–212 (2013).

[58] L. Van der Maaten and G. Hinton, "Visualizing data using t-SNE," J. Mach. Learn. Res. **9**, 2579 (2008).